International Journal of Remote Sensing
Vol. 31, No. 15, 10 August 2010, 4217–4226

Taylor & Francis
Taylor & Francis Group

A two-stage method for oil slick segmentation

FANG LI† and CHAOMIN SHEN‡*
†Department of Mathematics, East China Normal University, Shanghai, China
‡Department of Computer Science, East China Normal University, Shanghai, China

(*Received 19 January 2007; in final form 14 December 2008*)

In this paper we propose a two-stage algorithm for oil slick segmentation in synthetic aperture radar (SAR) images. In the first stage, we propose a new variational model to reduce speckles in non-textured SAR images. Applications to simulated and real SAR images show that the method is well balanced in the quality of the conventional criteria. Then, in the second stage, we use the fast Chan–Vese (CV) model and the level set method to segment the oil slick in the de-speckled SAR image. The additive operator splitting (AOS) scheme is used in the numerical implementation to improve computational efficiency. Experimental results show that our two-stage algorithm is effective for oil slick segmentation in SAR images.

1. Introduction

Synthetic Aperture Radar (SAR) images have been widely used for environmental monitoring, including oil slick detection. However, the imagery produced by SAR systems suffers from the effects of speckle noise. In SAR images, an oil slick appears as a dark slick or spot, whereas the surrounding water appears bright. The SAR images with oil slicks are usually non-textured and have a high noise and low contrast, disturbing their extraction and analysis.

To reduce speckles, several geometric filters, such as the Enhanced Lee, the Enhanced Frost and the Gamma filters (Lopes *et al.* 1993), are utilized. Furthermore, some variational de-speckling models are also introduced such as the Rudin–Lions–Osher (RLO) model (Rudin *et al.* 1994, 2003).

This paper focuses on the segmentation of an oil slick in SAR images using a two-stage method. In the first stage, we propose a variational model to reduce speckles in non-textured SAR images based on the RLO model. In the second stage, the de-speckled oil slick image is segmented. For segmentation, we make use of the implicit active contour model which has been widely used in image segmentation and object tracking. The implicit active contour model involves the level set method. The idea is to view the active contour as a zero level set of an evolving surface driven by partial differential equations (PDEs) (Sethian 1996). As the surface evolves, the active contour changes. Then the final contour is extracted when the evolution stops. The main advantages of the implicit active contour model are the automatic handling of topology changes, high numerical stability and independence of parametrization. However, the main drawback is the additional computational complexity. In order to overcome this drawback, special techniques, such as the narrow band and additive operator splitting

*Corresponding author. Email: cmshen@cs.ecnu.edu.cn

International Journal of Remote Sensing
ISSN 0143-1161 print/ISSN 1366-5901 online
http://www.tandf.co.uk/journals
DOI: 10.1080/01431160903193513

(AOS) scheme, are introduced. The Chan–Vese (CV) model (Chan and Vese 2001) is one of the basic implicit active contour models. PDEs and the level set method have been introduced in oil slick segmentation by Huang *et al.* (2005). In this paper, we use the fast CV model which is a modification of the original CV model to segment the oil slicks.

The present paper is organized as follows: in section 2, we propose the de-speckling model for SAR images. The algorithm is compared with classical de-speckling filters and the RLO model using both simulated and real SAR images. In section 3, we explain the fast CV model and its level set evolution equation. In section 4, we explain the numerical implementation with the AOS scheme. Then we test the two-stage method on two real SAR images for oil slick segmentation in section 5. Finally, we conclude our paper in section 6.

2. SAR image de-speckling model

2.1 *The proposed model*

Speckle noise in SAR images is modelled as a multiplicative noise process. Assume that the true radiometric value of the image is represented by u, the intensity value measured by the SAR system is u_0, and the speckle noise is n. Then the speckle noise model is given by:

$$u_0 = un. \tag{1}$$

For one-look SAR images, n is negative exponentially distributed with mean one. For multi-look SAR images, n follows the Gamma distribution with mean one. For the details of SAR's multiplicative noise model, see Oliver and Quegan (1998).

Based on equation (1) and the well-known Rudin-Osher-Fatemi (ROF) model (Rudin *et al.* 1992), the RLO model (Rudin *et al.* 1994, 2003) considers the following constrained minimization problem:

$$\begin{aligned} &\min\left\{E(u) = \textstyle\int_\Omega |\nabla u| \mathrm{d}x\right\} \\ \text{subject to } &\textstyle\int_\Omega \left(\frac{u_0}{u} - 1\right)\mathrm{d}x = 0, \quad \int_\Omega \left(\frac{u_0}{u} - 1\right)^2 \mathrm{d}x = \sigma^2. \end{aligned} \tag{2}$$

The RLO model used the assumption that the noise has mean 1 and standard deviation σ. It is solved by the Lagrange multiplier method, and the two Lagrange multipliers are updated in the evolution process.

Chan and Esedoglu (2005) claimed that for the removal of Gaussian noise, using the L^1 norm fidelity term has the advantages of having more geometric information and maintaining good contrast. That encourages us to use an L^1 norm fidelity term in the de-speckling case. Then we propose the following energy minimization model:

$$\min_{u \in BV(\Omega)} \left\{ E(u) = \int_\Omega |\nabla u| \mathrm{d}x + \lambda \int_\Omega \left| \frac{u_0}{u} - 1 \right| \mathrm{d}x \right\}, \tag{3}$$

where BV denotes the bounded variation space. Unlike the RLO model, equation (3) is an unconstrained problem with only one fidelity term. λ is a user defined parameter. In this paper, we focus on the de-speckling of almost piecewise constant images. Although the RLO model has a similar performance to the proposed model, the proposed model is simpler than the RLO model both in the formulation and implementation. Moreover, our model is more stable than the RLO model in the de-speckling process. Hence the proposed model is more suitable for our oil slick segmentation problem.

Experiments show that in the proposed model λ should be chosen in the range [1, 100]. However, in the RLO model, when the noise level is high, the two Lagrange multipliers vary dramatically, causing instability of the algorithm. By the standard argument in the variational method, we get the associated Euler–Lagrange equation of (3):

$$\begin{cases} -\operatorname{div}\left(\dfrac{\nabla u}{|\nabla u|}\right) - \lambda \dfrac{u_0(u-u_0)}{u^2|u-u_0|} = 0, & \text{in } \Omega \\ \dfrac{\partial u}{\partial N} = 0, & \text{on } \partial\Omega \end{cases} \tag{4}$$

where N is the unit outward normal of $\partial\Omega$. Using the steepest descent method, we get the associated heat flow

$$\begin{cases} u_t = \operatorname{div}\left(\dfrac{\nabla u}{|\nabla u|}\right) + \lambda \dfrac{u_0(u-u_0)}{u^2|u-u_0|}, & \text{in } \Omega \times \mathbb{R}^+ \\ u|_{t=0} = u_0, & \text{in } \Omega \\ \dfrac{\partial u}{\partial N} = 0. & \text{on } \partial\Omega. \end{cases} \tag{5}$$

2.2 *Evaluation of results*

We compare our algorithm with the Enhanced Lee filter, the Enhanced Frost filter, the Gamma filter and the RLO model in what follows using a simulated and a real SAR image. We select the parameters for each method by trial-and-error in order to achieve optimal results.

For the simulated SAR image, since the true image (piecewise smooth, non-textured) is known, the indices such as the Mean Absolute Error (MAE), the Mean Square Error (MSE) and the Signal-to-Noise-Ratio (SNR) are used as criteria to evaluate the de-speckling algorithm (Schulze and Wu 1995). However, for the real SAR image, the conventional evaluation criteria include edge preservation, mean preservation, reduction of standard deviation and visual appearance (Han *et al.* 2002).

Table 1 shows that the proposed method has the lowest MSE and the highest SNR among all algorithms except that the MAE is a little higher than the RLO model. By these indices, we conclude that our proposed model and the RLO model are superior to other filters. In figure 1, we display the results of the five algorithms. The filters are applied with window size 5×5. In visual appearance, the de-speckled images by the RLO model (figure 1(*f*)) and our method (figure 1(*g*)) are closest to the true image (figure 1(*a*)) while the other filters blur the edges (figures 1(*c*)–(*e*)).

For the European Remote-Sensing Satellite (ERS)-2 Precision Image (PRI), the RLO model is not stable since the noise level is high, and then the two Lagrange multipliers vary significantly and their values are either very big or very small. For this image, the filters are applied with window size 7×7. Figure 2 shows that the proposed model is powerful in terms of edge preservation and speckle removal. From table 2, we find that the proposed model, the Enhanced Lee filter and the Gamma filter, except the Enhanced Frost filter, can well preserve the global mean. The Edge Preservation Index (EPI) (Huang *et al.* 2005) is used to compare the results. The larger the value of EPI, the greater degree of edge preservation. Table 2 shows that the proposed model has a higher EPI than the Enhanced Lee filter and the Gamma filter. When the iteration is 15, the EPI of the proposed model is the highest. In visual appearance,

Table 1. Comparison of de-speckling ability on a simulated SAR image.

Algorithm	MAE	MSE	SNR(dB)
None (Simulated SAR image)	20.04	568.68	6.20
Enhanced Lee filter			
3×3	23.85	923.72	4.09
5×5	25.38	1.09×10^3	3.37
7×7	27.36	1.29×10^3	2.63
Enhanced Frost filter			
3×3	30.78	1.90×10^3	0.96
5×5	41.57	3.29×10^3	–1.43
7×7	45.84	4.01×10^3	–2.28
Gamma filter			
3×3	30.26	1.51×10^3	1.95
5×5	29.33	1.48×10^3	2.04
7×7	29.02	1.47×10^3	2.08
RLO model	4.55	89.80	14.21
Proposed model	4.66	89.73	14.22

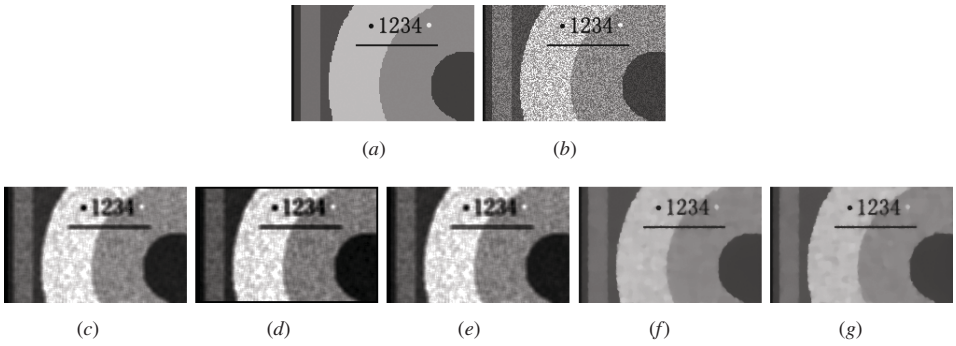

Figure 1. Comparison of different de-speckling algorithms using a simulated SAR image. (*a*) The true noise-free image with size 196 by 124; (*b*) the simulated SAR image (by the Matlab program); (*c*) result of the Enhanced Lee filter; (*d*) result of the Enhanced Frost filter; (*e*) result of the Gamma filter; (*f*) result of the RLO model with iteration 20; (*g*) result of the proposed model with iteration 20.

our proposed model can better preserve the edges while the results of the filters are somewhat blurring.

Two sub-areas labelled as I and II (20 by 20 pixels each) taken from the ERS-2 PRI and the smoothed images in figure 2 are chosen for evaluating the reduction of standard deviation (SD) and mean (Mean) preservation. Table 2 shows that the proposed model can preserve the mean in area I as good as other filters. Meanwhile, it can better preserve the mean in area II. The standard deviation of the proposed model is lower than the filters except in area I when the iteration is 15. As far as the proposed model is considered, as the iterations increase, the mean index increases slowly, but the standard deviation decreases rapidly. On the whole, from the above analysis, the proposed model can effectively preserve the image mean and edges, as well as reduce the standard deviation. So it is a powerful de-speckling algorithm.

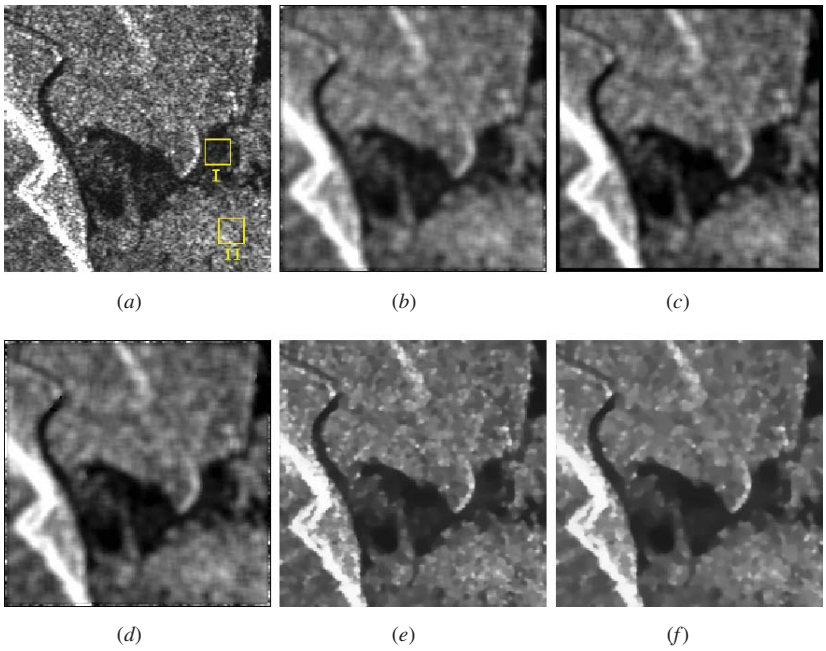

Figure 2. ERS-2 PRI image (Photo: ESA, Acquired: 09-APR-2000 Center: S20:37:46/ E149:11:23) over the Proserpine area in Queensland, Australia is used to demonstrate the de-speckle algorithms. (*a*) ERS-2 PRI with size 200 by 200; (*b*) result of the Enhanced Lee filter; (*c*) result of the Enhanced Frost filter; (*d*) result of Gamma filter; (*e*) result of the proposed model with iteration 15; (*f*) result of the proposed model with iteration 20.

Table 2. Comparison of de-speckling ability on a real SAR image.

Algorithm	Mean	EPI	Area I Mean	Area I SD	Area II Mean	Area II SD
None (SAR image)	2.64×10^4		1.17×10^4	4.44×10^3	3.22×10^4	6.26×10^3
Enhanced Lee filter	2.64×10^4	0.24	1.16×10^4	2.12×10^3	3.37×10^4	3.71×10^3
Enhanced Frost filter	2.49×10^4	0.30	1.16×10^4	2.12×10^3	3.37×10^4	3.71×10^3
Gamma filter	2.64×10^4	0.24	1.16×10^4	2.12×10^3	3.37×10^4	3.71×10^4
Proposed (iter = 15)	2.64×10^4	0.36	1.16×10^4	2.23×10^3	3.28×10^4	3.52×10^3
Proposed (iter = 20)	2.64×10^4	0.29	1.16×10^4	1.81×10^3	3.31×10^4	3.33×10^3

In figures 1 and 2, for the proposed model, the equation 5 is implemented with the AOS scheme (see section 4) with $\lambda = 10$ and time step $\tau = 1$.

3. Fast CV model

Let $u_0 : \Omega \subset \mathbb{R}^2 \to \mathbb{R}$ be a given gray scale image, and $C(s) : [0, 1] \to \mathbb{R}^2$ be a parametrized curve. Chan and Vese (2001) proposed the following minimization method for two-phase segmentation:

$$\begin{aligned} \min\{E(C, c_1, c_2) = \mu \textstyle\int_0^{L(C)} \mathrm{d}s + \nu \int_{\mathrm{inside}(C)} \mathrm{d}A \\ + \lambda_1 \textstyle\int_{\mathrm{inside}(C)} |u_0 - c_1|^2 \mathrm{d}x + \lambda_2 \int_{\mathrm{outside}(C)} |u_0 - c_2|^2 \mathrm{d}x\} \end{aligned} \tag{6}$$

where $L(C)$ is the arc length of the curve C, and $\mu \geq 0$, $\nu \geq 0$, λ_1, $\lambda_2 \geq 0$ are fixed parameters. The first term is a length term that makes the active contour have some regularity and not fractal. The second term is called the balloon force term used to adjust the moving speed of the curve in the normal direction. The last two terms can be seen as the fidelity terms.

In the level set method (Sethian *et al.* 1996), $C \subset \Omega$ is represented by the zero level set of a Lipschitz function $\phi : \Omega \to \mathbb{R}$, such that

$$\begin{cases} C = \{x \in \Omega : \phi(x) = 0\}, \\ \text{inside}\,(C) = \{x \in \Omega : \phi(x) > 0\}, \\ \text{outside}\,(C) = \{x \in \Omega : \phi(x) < 0\}. \end{cases} \tag{7}$$

In the level set formulation, the CV model is expressed as

$$\begin{aligned} \min\{E(\phi, c_1, c_2) = \mu \textstyle\int_\Omega \delta(\phi)|\nabla\phi|\mathrm{d}x + \nu \int_\Omega H(\phi)\mathrm{d}x \\ + \lambda_1 \textstyle\int_\Omega |u_0 - c_1|^2 H(\phi)\mathrm{d}x + \lambda_2 \int_\Omega |u_0 - c_2|^2 (1 - H(\phi))\mathrm{d}x\}. \end{aligned} \tag{8}$$

Here ϕ is the level set function, $H(\phi)$ is the Heaviside function: $H(\phi) = 1$ if $\phi \geq 0$ and $H(\phi) = 0$ otherwise, and $\delta(\phi)$ is the Dirac function. The minimization of equation (8) is achieved by introducing an artificial time variable, and moving in the steepest direction to steady state

$$\begin{cases} \phi_t = \delta_\varepsilon(\phi)\left[\mu \mathrm{div}\left(\frac{\nabla\phi}{|\nabla\phi|}\right) - \nu - \lambda_1(u_0 - c_1)^2 + \lambda_2(u_0 - c_2)^2\right], & \text{in } \Omega \times \mathbb{R}^+ \\ \phi(0, x) = \phi_0(x), & \text{in } \Omega \\ \dfrac{\delta_\varepsilon(\phi)}{|\nabla\phi|}\dfrac{\partial\phi}{\partial n} = 0, & \text{on } \partial\Omega \end{cases} \tag{9}$$

where $\delta_\varepsilon(\phi)$ is an approximation of $\delta(\phi)$ and c_1, c_2 are updated by the formula

$$c_1 = \frac{\int_\Omega u_0 H(\phi)\mathrm{d}x}{\int_\Omega H(\phi)\mathrm{d}x}, \quad c_2 = \frac{\int_\Omega u_0(1 - H(\phi))\mathrm{d}x}{\int_\Omega (1 - H(\phi))\mathrm{d}x}. \tag{10}$$

The advantage of the CV model is that it can detect the interior boundary and the boundaries are not necessarily defined by gradient. It is perfect in the segmentation of piecewise constant or piecewise smooth images. However, the CV model is not very efficient when dealing with image of large size or high noise. The oil slicks in our de-speckled SAR images are piecewise smooth dark regions without explicit edges, hence the CV model is quite suitable to segment such images. Moreover, inspired by Zhao *et al.* (1996), we replace the factor $\delta_\varepsilon(\phi)$ in (8) by $|\nabla\phi|$ in order to improve the convergence speed. Then we obtain the so-called fast CV model:

$$\begin{cases} \phi_t = |\nabla\phi|\left[\mu \mathrm{div}\left(\frac{\nabla\phi}{|\nabla\phi|}\right) - \nu - \lambda_1(u_0 - c_1)^2 + \lambda_2(u_0 - c_2)^2\right], & \text{in } \Omega \times \mathbb{R}^+ \\ \phi(0, x) = \phi_0(x), & \text{in } \Omega \\ \dfrac{\delta_\varepsilon(\phi)}{|\nabla\phi|}\dfrac{\partial\phi}{\partial n} = 0, & \text{on } \partial\Omega \end{cases} \tag{11}$$

where c_1 and c_2 are updated by the formula (6). This algorithm is stable and very efficient in segmenting the noise-free image or low noise image with piecewise smooth features.

4. Numerical implementation and the AOS scheme

Here we use the AOS scheme (Weickert *et al.* 1998) to implement equations (5) and (11). First we rewrite the evolution equations (5) and (11) in a uniform formula as

$$\begin{aligned} v_t &= \alpha(v)\,\mathrm{div}\,(g\nabla v) + \eta(v) \\ &= \alpha(v)\frac{\partial}{\partial x_1}\left(g(x)\frac{\partial}{\partial x_1}v\right) + \alpha(v)\frac{\partial}{\partial x_2}\left(g(x)\frac{\partial}{\partial x_2}v\right) + \eta(v). \end{aligned} \tag{12}$$

Denoting

$$A_1 = \frac{\partial}{\partial x_1}\left(g(x)\frac{\partial}{\partial x_1}\right), \quad A_2 = \frac{\partial}{\partial x_2}\left(g(x)\frac{\partial}{\partial x_2}\right), \tag{13}$$

we can write the evolution equation as

$$v_t = \alpha(v)\,(A_1 + A_2)v + \eta(v). \tag{14}$$

We employ discrete times $t_n = n\tau$, where $n \in N$ and τ denotes the time step size. Additionally, an image is divided into grid nodes (i, j) by a uniform mesh of spacing h. Using standard notation, v_{ij}^n denotes the approximation of $v(ih, jh, t_n)$. As Weickert *et al.* (1998), we use a simple discretization for the A_l, $l \in \{1,2\}$ operators. For example, we can write A_1 as follows: Rearrange the image matrix row by row as one column and let

$$\frac{\partial}{\partial x_1}\left(g(x)\frac{\partial}{\partial x_1}v\right) \approx \sum_{j\in N(i)} \frac{g_j + g_i}{2h^2}\,(v_j - v_i), \tag{15}$$

where $N(i)$ is the set $\{i-1, i+1\}$, representing the two horizontal neighbours of pixel i. The elements of A_1 are thereby given by

$$a_{ij} = \begin{cases} \dfrac{g_i + g_j}{2h^2}, & j \in N(i) \\ -\displaystyle\sum_{k\in N(i)} \dfrac{g_i + g_k}{2h^2}, & j = i \\ 0 & \text{else.} \end{cases} \tag{16}$$

Then the AOS scheme gives the iteration

$$v^{n+1} = \frac{1}{2}\sum_{l\in\{1,2\}} (I - 2\tau\alpha(v^n)A_l(v^n))^{-1}(v^n + \eta(v^n)) \tag{17}$$

where I denotes the unit matrix. Since the time step τ should be chosen as large as in the interval [1, 10], the AOS scheme is very efficient.

Note that the boundary conditions of (5) and (11) are satisfied by extending the boundary value of the initial data u_0 and the initial level set ϕ_0 symmetrically.

5. Application to oil slick segmentation

The following Environmental Satellite (ENVISAT) Advanced Synthetic Aperture Radar (ASAR) image shows the oil slick released by a crippled tanker in the north-west coast of Spain in 2002. The tanker itself is visible as a white dot at the bottom-left of the oil slick.

In figure 3, the speckle noise in the ENVISAT ASAR image is perfectly suppressed. In the de-speckled image, the oil slick has piecewise smooth dark features. Therefore,

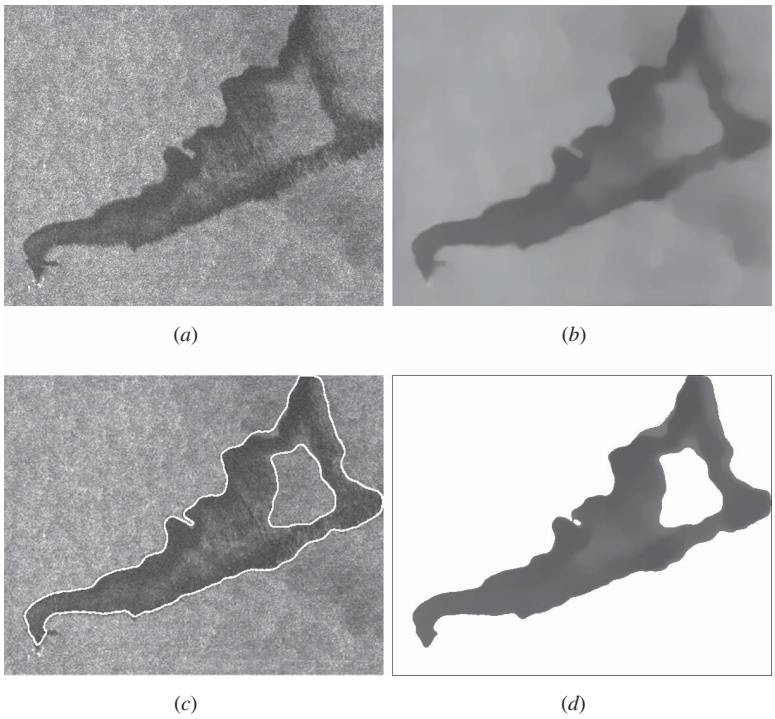

Figure 3. An ENVISAT ASAR image (Photo: ESA, Orbit: 3741; Track: 180) of the Spanish coast is used to demonstrate the proposed two-stage oil slick segmentation algorithms. (*a*) ENVISAT ASAR image with size 600 by 476; (*b*) the de-speckling result by the proposed model (parameters: $\tau = 5$, $\lambda = 10$, iteration $= 20$); (*c*) the oil slick segmentation result by the fast CV model (parameters: $\tau = 5$, $\mu = 1$, $\lambda_1 = 3$, $\lambda_2 = 1$, $\nu = 0$, iteration $= 20$); (*d*) threshold segmentation result based on the de-speckled image.

the fast CV model can successfully segment the oil slick; especially the interior boundary is delineated out. Threshold segmentation based on the de-speckled image shows good results too. The threshold is set to be the median value of the de-speckled image. However, with a close look, there are some isolated points around the boundaries, which is not so satisfactory.

In figure 4, the ERS-2 SAR image suffers from speckle noise. It is de-speckled into a piecewise smooth image such that the oil slick is easy to be delineated out by the fast CV algorithm. In the threshold segmentation result, there is a hole in the bottom of the left oil part which is really oil. The result of the fast CV algorithm is more exact.

For the above two images, the computation time for each stage is several seconds since fewer than 20 iterations are needed. Both segmentation results are satisfactory in terms of visual appearance. Compared with other segmentation methods such as intensity threshold, our two-stage method is highly automatic and the extracted oil slick boundaries are smooth.

6. Conclusion

Speckles in SAR images disturb the analysis of SAR images. In this paper, we have proposed a two-stage algorithm for oil slick segmentation in SAR images. Firstly, we de-speckled the SAR image with a new variational model. This de-speckling

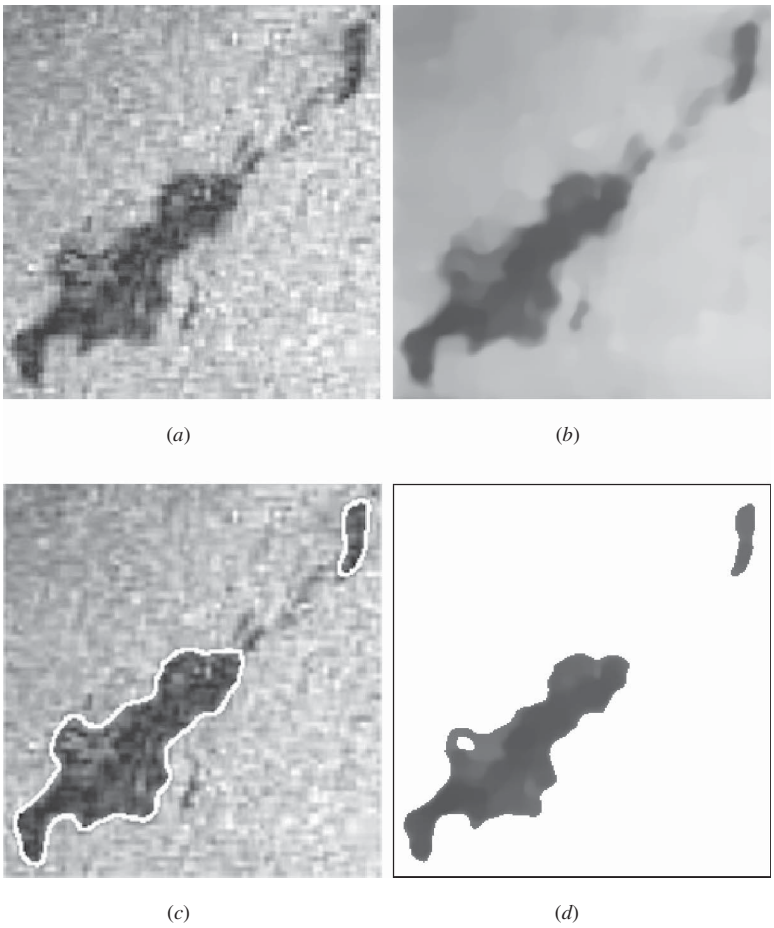

Figure 4. An ERS-2 SAR image of the Caspian Sea (Photo: ESA) is used to demonstrate the proposed two-stage oil slick segmentation algorithms. (*a*) ERS-2 SAR image with size 250 by 260; (*b*) the de-speckling result by the proposed model (parameters: $\tau = 5$, $\lambda = 10$, iteration $= 20$); (*c*) the oil slick segmentation result by fast CV model (parameters: $\tau = 5$, $\mu = 1$, $\lambda_1 = 1.3$, $\lambda_2 = 1$, $\nu = 0$, iteration $= 10$); (*d*) threshold segmentation result based on the de-speckled image.

algorithm is powerful, judged by the conventional criteria, especially for the case that the regions of interest are piecewise smooth (non-textured) such as a SAR image with oil slick features. In other cases, where texture or strong targets are dominating, this method processes less well, since there is a trade-off between speckle reduction and small-scale feature preservation. By the de-speckling algorithm, the SAR images with oil spills are processed into piecewise smooth images. Then in the second stage, a fast CV model is utilized to delineate out the oil slicks. The algorithm only costs several seconds in each stage, so it is of high efficiency.

Acknowledgements

This work is partially supported by the National Science Foundation of China (60773119, 10971066), the National Science Foundation of Shanghai (10ZR1410200) and the Research Fund for the Doctoral Program of Higher Education

(200802691037). The authors are grateful to the anonymous referees for helpful suggestions.

References

CHAN, T. F. and ESEDOGLU, S., 2005, Aspects of total variation regularized L1 function approximation. *SIAM Journal on Applied Mathematics*, **65**, pp. 1817–1837.

CHAN, T.F. and VESE, L.A., 2001, Active contour without edges. *IEEE Transactions on Image Processing*, **10**, pp. 266–277.

HAN, C.M., GUO, H.D., WAN, C.L. and FAN, D., 2002, A novel method to reduce speckle in SAR images. *International Journal of Remote Sensing*, **23**, pp. 5095–5101.

HUANG, B., LI, H. and HUANG, X., 2005, A level set method for oil slick segmentation in SAR images. *International Journal of Remote Sensing*, **26**, pp. 1145–1156.

LOPES, A., NEZRY, E., TOUZI, R. and LAUR, H., 1993, Structure detection and statistical adaptive speckle filtering in SAR images. *International Journal of Remote Sensing*, **14**, pp. 1735–1758.

LOPES, A., TOUZI, R. and NEZRY, E., 1990, Adaptive speckle filters and scene heterogeneity. *IEEE Transactions on Geoscience and Remote Sensing*, **28**, pp. 992–1000.

OLIVER, C. and QUEGAN, S., 1998, *Understanding Synthetic Aperture Radar Images*, p. 98 (Boston: Artech House).

RUDIN, L.I., LIONS, P.L. and OSHER, S., 2003, Multiplicative denoising and deblurring: Theory and algorithms. In *Geometric Level Sets in Imaging, Vision, and Graphics*, S. Osher and N. Paragios (Eds.), pp. 103–119 (New York: Springer-Verlag).

RUDIN, L.I. and OSHER, S., 1994, Total variation based image restoration with free local constraints, *Proceedings ICIP-94, IEEE International Conference*, **1**, pp. 31–35.

RUDIN, L.I., OSHER, S. and FATEMI, E., 1992, Nonlinear total variation based noise removal algorithms. *Physica D: Nonlinear Phenomena*, **60**, pp. 259–268.

SCHULZE, M. and WU, Q.X., 1995, Nonlinear edge-preserving smoothing of Synthetic Aperture Radar images. *Proceedings of New Zealand Image and Vision Computing '95 Workshop*, August 1995, Christchurch, New Zealand, pp. 65–70.

SETHIAN, J.A., 1996, *Level Set Methods: Evolving Interfaces in Geometry, Fluid Mechanics, Computer Vision and Materials Sciences* (Cambridge: Cambridge University Press).

WEICKERT, J., ROMENY, B.M.T.H. and VIERGEVER, M.A., 1998, Efficient and reliable scheme for nonlinear diffusion filtering. *IEEE Transactions on Image Processing*, **7**, pp. 398–410.

ZHAO, H.K., CHAN, T.F., MERRIMAN, B. and OSHER, S., 1996, A variational level set approach to multiphase motion. *Journal of Computer Physics*, **127**, pp. 179–195.